Small 8 (15), 2436-2444

Investigation of analyte-induced multicomponent rod aggregation using tunable pores

Mark Platt, Geoff R. Willmott and Gil U. Lee**

[*] Dr. M. Platt, Prof. G. U. Lee.

School of Chemistry and Chemical Biology, University College Dublin, Belfield, Dublin 4, D4. Ireland

mark.platt@ucd.ie or gill.lee@ucd.ie

Dr. G. R. Willmott

Industrial Research Limited, 69 Gracefield Rd, PO Box 31-310, Lower Hutt 5040, New Zealand.

The MacDiarmid Institute for Advanced Materials and Nanotechnology.

Supporting Information is available under http://www.small-journal.com or from the author.

Keywords: **Tunable pores, multicomponent rods, aptamer, agglutination, platelet derived growth factor**

Abstract

Tunable nanopores, *TPs,* are used to monitor individual and aggregated rod shaped nanoparticles as they move through a membrane opening. By comparing particles of similar dimensions, we demonstrate that the resistive pulse signal from a rod is fundamentally different to that of a sphere. Rods can be distinguished using two measurements, the blockade event magnitude Δi_p, which reveals the particle's size, and the full width half maximum, *FWHM*, which relates to the rod length. While the observed Δi_p values agree well with

simulations, the measured FWHM times are much larger than expected. This increased dwell time, caused by rods moving through the pore in various orientations, is not observed for spherical particles. These differences were exploited in a new agglutination assay using rod shaped particles. By controlling the surface chemistry and the location of the capture ligand, rods were made to form either long "end-on-end" or wide "side-on" aggregates upon the addition of an analyte. This observation will facilitate multiplexed detection, as particles with a particular aspect ratio particle can be distinguished by two measurements. We demonstrate the assay's potential with the detection of platelet derived growth factor, PDGF-BB, using an aptamer capture probe resulting in sensitivity down to femtomolar levels.

1. Introduction

The characterization of colloid and nanoparticle based systems has been aided in recent years by the resurgence and development of Coulter counting and micro- to nanopore based technologies[1-9]. Collectively known as resistive pulse sensing, *RPS*, they offer an attractive technology format because the measurements provide information on individual particles within their natural environment. RPS has been used to study numerous types of particles, including single molecules, proteins, biological[3, 10, 11] and synthetic nanoparticles[6, 9]. Pores typically fall into two categories, biological or solid state. Biological nanopores such as α-haemolysin, which has a diameter of 1.4 nm at its narrowest point, have been used to detect and observe ssDNA[12-14]. Whilst biological pores offer an insight into single molecules and cellular mechanisms, their fixed size, long-term stability and compatibility in systems with variable pH, ionic strength and temperatures can limit their applications. Solid-state nanopores often support more chemical versatility, but have fixed pore diameters with carbon nanotubes[4, 5, 7], PDMS[15], glass[1, 16, 17], silicon[3] and polycarbonate[10, 18] used as substrates.

Recently, tunable elastomeric pore technologies have emerged[8, 11], allowing further versatility as the pore can be stretched in real time to suit the sample[6, 19]. Tunable pores, *TP*s, are fabricated by mechanically puncturing a thermoplastic polyurethane membrane[11, 20]. The membrane can be stretched in a controlled, reversible fashion to change the pore geometry – altering the size of the pore by as much as an order of magnitude[21]. Techniques have been developed for using TPs to accurately determine the concentration[9], size[6] and surface charge[22] of dispersed inorganic particles. They are capable of detecting biological particles[6, 11, 20, 23] as well as discriminating between particles of different functionalization[19, 24]. TPs are typically used to measure particles with one dimension larger than 100 nm, making them suitable for a wide range of applications[8], and detailed studies of resistive pulse shapes, could allow studies into particle morphology[25].

In RPS experiments, the TP is filled with a conducting medium, and a potential is applied between two electrodes on either side of the pore opening. This establishes a current flow through the pore, known as a base line current (i_p), which is proportional to the applied voltage and electrolyte conductivity. Previous work has discussed analytical[6, 8, 9] and semi-analytical[6, 25, 26] descriptions of the baseline current in TPs, and the current change caused when a particle moves through a pore (Δi_p, Figure 1). For a simple cylindrical pore, the latter is given by[4, 5],

$$\frac{\Delta i_p}{i_p} = \frac{S\left(d_p, d_s\right)\left(d_s^3\right)}{\left(l_p + 0.8 d_p\right) d_p^2} \qquad (1)$$

where l_p is the pore length, d_p is the pore diameter, d_s is the diameter of a spherical particle, and $S(d_p,d_s)$ is a correction factor that depends on d_p and d_s. Although TPs are conical, the proportionality between Δi_p and particle volume in Equation (1) still holds to a good degree of accuracy, and can be used for particle sizing[6]. Particle size is one of two measurements used for this study, the second being full width half maximum, FWHM, which is an indication of

time taken for the particle to traverse the pore. The velocity of the particle is given by the sum of the contributions from pressure driven flow, $\upsilon_{s,PD}$, electrophoresis, $\upsilon_{s,EP}$, electroosmosis, $\upsilon_{s,EO}$ and diffusion, $\upsilon_{s,D}$, and in the present work is dominated by pressure-driven flow, as P1>P2 (Figure 1a).

Nanoparticles with magnetic properties are increasingly being used in diagnostic assays, either to aid sample purification[27-29] or to facilitate detection[30-33]. One simple detection strategy utilizes an analyte's capacity to simultaneously bind to multiple particles leading to aggregation[29, 32, 34-36]. In agglutination assays, the concentration of the analyte is inferred from the changes in aggregate size or frequency. This simple strategy has been used in conjunction with cytometry[31], colorimetry[37, 38], magneto resistive sensing[39], and dynamic light scattering detection platforms[32, 34]. Particles are typically synthesized with dual functionality i.e. an optical property for detection and a magnetic component to aid separation[40, 41], and particle synthesis routes are numerous, from Janus-particles[42-45] to core shell configurations[46, 47]. Electrodeposition within a template offers an alternative route to producing particles[33, 48-52], as the particles can be synthesized to contain several materials giving the appearance of a barcode[40, 51]. Rod shaped particles offer an intriguing advantage over spheres in agglutination assays, as rods have two physical dimensions which can be changed, diameter and length. Rods of varying aspect ratios can be assigned to capture an analyte, and the frequency of their aggregates counted. Additionally rods have also been shown to aggregate in different configurations: end-to-end[53], or forming rafts[54].

We present the first published measurements of rod shaped particles using a TP, and demonstrate that a clear and reproducible signal can be observed. We characterize and model the signal from the particles as they traverse the pore and relate Δi_p to the size of the particle. The data suggests that the FWHM is related to the rod length, and indicate that the particles traverse the pore in various orientations. Utilizing both measurements, an agglutination assay

was designed and demonstrated using two capture probes, the model biotin-avidin system and a DNA aptamer system. Aptamers are oligonucleotide or peptide sequences that are capable of binding to targets with high specificity and selectivity[55-57]. Their lower production costs and the range of analytes to which they can bind make them an attractive alternative to antibodies. The aptamer chosen here is the 35mer sequence which binds to the protein platelet derived growth factor, PDGF-BB, with a $K_d \sim 0.1$ nM[37]. The ability to detect PDGF is of interest as it is one of numerous growth factors over expressed in the serum of cancer patients, particularly those with lung and pleural tumors. Here the aggregation of rods is used to detect the PDGF protein down to fM levels of sensitivity with an assay time on the order of 10 minutes.

2. Results and discussion

Template deposition produces particles with dimensions that are controlled by both the reaction time, and the template itself. Pores within the Al_2O_3 membrane used have an average diameter of circa 300 nm, which determines the diameter of the growing particle. The length of the rod is determined by the total charge passed (Figure 2). The composition of material within the rod can be controlled by varying the plating solution as well as the potential under which the reaction takes place[49].

2.1 TP optimization.

Prior to performing an assay, Au rods of varying lengths (Figure S1) were synthesized to act as a set of control particles and aid the study of rod shaped particles as they traverse a TP. One unique property of the system is the ability to stretch and relax the pore membrane, which can alter the inferred pore size by an order of magnitude[21] and is described in detail elsewhere[9, 11, 21]. The membrane stretch is quantified by the increased separation of actuation points on a macroscopic pore specimen, additional to the separation of approximately 41.5

mm when the membrane is unstretched. A series of optimization experiments were performed to study the signal from cylindrical particles traversing the pores across a range of membrane stretches. This ensured that a pore size and potential (Figure S2) could be selected to produce a clear signal. The measurements (Figure 3) record Δi_p and FWHM as the membrane stretch is increased. Two sets of calibration spheres, 0.955 μm and 2 μm in diameter, and rods composed of Au, 2.1 μm and 4.7 μm in length were used (Figure S1).

In Figure 3A, Δi_p decreases for the spherical particles as the membrane stretch is increased, matching previous observations for similar systems[19], and is consistent with Equation 1. In contrast, Δi_p appears to be constant or slightly increased for the rods . As the pore size increases, the rods are more likely to be tilted with respect to the pore axis. Tilted rods will displace a greater volume of electrolyte near the pore constriction when the peak current change is measured, producing an increase in pulse size.

2.1.1 Simulated Δi_p and FWHM

Simulated resistive pulses in Figure 4 were carried out using a semi-analytic model described elsewhere[6, 9, 22, 26]. Briefly, the model assumes conical pore geometry with a symmetric constriction close to the membrane surface containing the smaller pore opening (Figure 1A). Simulations were calibrated using the X = 2.5 mm experiment for 955 nm spheres at 0.12 V, matching the baseline current, as well as typical pulse magnitude, duration, and asymmetry. The resulting fitted parameters were 168.5 Pa across the membrane, with pore opening radii 14.6 and 2.1 micron, and a constriction 4.1 micron below the pore surface. Simulated resistive pulses for rods assume that the rod is not tilted.

Figure 4 shows that although Δi_p is predicted to vary by more than an order of magnitude between the four particle sets, the experimental variation is very close to the predicted response. The predicted and measured Δi_p and FWHM values at 2.5 mm stretch and 0.12V are

listed in Table 1, the largest deviation from the simulated values occurs for the FWHM of the longer 4.7 μm rods. It is clear from Figure 3B that across all stretches the two rod shaped particles produce a FWHM value larger than the spherical beads, with 4.7 μm long rods recording the largest FWHM values, which implies the longest translocation time.

*2.1.2. Demonstration assay***.**

A control experiment was performed to determine the sensitivity of the TP to solutions containing mixtures of the 2.1 μm and 4.7 μm Au rods, Figure 5. Initially a solution containing only 2.1 μm rods was analyzed. The mole fraction of the 4.7 μm rod was then increased from 0 to 100%. Modal Δi_p (Figure 5A) and FWHM (Figure 5B) values are plotted as a percentage change from the initial 2.1 μm value. The measured values for Δi_p matched the simulated results reasonably well (dashed lines). FWHM values increase with the increasing fraction of 4.7 mm rods, and whilst the simulated results match this trend, they significantly underestimate the experimental values.

2.2. Agglutination assay

2.2.1 Avidin-biotin assay.

The use of rod shaped particles for agglutination assays could result in the particles coming together in number of different configurations, resulting in trends within FWHM and Δi_p which are difficult to interpret. One solution is to control the orientation of aggregation. In the experiments outlined below, Ni was incorporated into the rods, either at the end of the rod or as a segment in the middle. This was done for two reasons, firstly to make handing the rods much easier during any surface chemistry modifications and subsequent wash stages as the rods could be separated from solution using a simple hand held magnet as opposed to

centrifugation. Secondly the Ni surface could act as a loci for the capture probe, producing a "sticky" Ni segment that captures the analyte and acts as the centre for aggregation.

A schematic of the rods used for the agglutination assays is shown in Figure 6. By controlling the orientation of the rods' aggregation, rods of the similar aspect ratios could be used to produce alternate signal responses in the presence of a target analyte, thus making agglutinations assays easier to multiplex with TPs. If the rods aggregated end-on-end, (Figure 6C), we would observe a simultaneous increase in Δi_p and FWHM, as opposed to rods aggregating in a side-on configuration (Figure 6D), where only a change in Δi_p is observed.

The capture probes were conjugated to the Ni surface using a His-modified peptide[33], using either EDC or SMCC chemistry, described below. Two different capture probes were conjugated to the rods, the first example used the avidin protein. To confirm the surface chemistry was as shown in the schematic, the Ni modified avidin particles were incubated for 5 minutes with a solution of biotinylated-FITC. A localized fluorescent signal confirmed its success, Figure 6B.

Figure S3 shows the B-H curve for the rods with a Ni segment. The particles have a residual net magnetization in the absence of an applied field; a consequence of this was slow aggregation of the particles if they were left in solution without sonication for periods longer than 30 minutes. Figure 7A shows the percentage change in Δi_p and FWHM for 1 μm rods, end functionalized with Ni, in a buffered solution. The solution was placed on a rotating wheel and sampled at 5 min intervals. A slight increase in Δi_p and FWHM was measured over 15 minutes. The result indicates that the Ni caused some nonspecific aggregation over short reaction times, however it occurs at a level low enough to not be the dominant signal during the aggregation in the presence of an analyte. Given that the calculated mutual diffusion coefficient for the rod was 5.6×10^{-8} cm^2s^{-1}[58-60], using a length and radius of 1 μm and 150 nm, and by using a concentration of particles circa 300-500 fM, a total assay time of

10 min was chosen. These conditions should allow sufficient time for the assay to be completed, given that the rate determining step of the diffusion of the analyte to the rods[31, 34]. The rods were sonicated and an aliquot was drawn from the stock solution, an equal volume of analyte solution was then added. At the start of each assay a blank was measured after 10 minutes, to allow the percentage change for FWHM and Δi_p to be calculated in subsequent samples. Figure 7B shows the percentage change in Δi_p and FWHM for an assay using end functionalized rods, where the Ni segment has been conjugated to avidin and the target protein was a biotinylated-BSA, which contained on average 9 biotins/ protein. The same rod sample was incubated with a non-biotinylated protein solution, and the resulting changes in Δi_p and FWHM are shown as dashed lines in Figure 7B. The absence of signal change for the non biotinyated target demonstrates that the rods are not non-specifically aggregating around the protein. A similar protocol was used for the rods containing a Ni segment in the middle of the rod, results are shown in Figure 7C.

2.2.2 PDGF assay.

We finally demonstrated the end-on-end assay format again for the detection of PDGF. It is known that the aptamer binds to the protein in a 2:1 ratio[37] and has previously been used in an agglutination assay using gold particles and a colorimetric detection mechanism[37]. As with the avidin example above, we observed an increase in both the Δi_p and FWHM, Figure 7D. A control assay for the same rods using a different protein (BSA) produced small changes in FWHM and Δi_p, (Figure 7D circled data points), demonstrating that the aggregation was not nonspecific.

3. Discussion

3.1 TP Optimization and Rod Orientation

End-on, axially symmetric rod orientation is a natural starting point for analysing and simulating rod resistive pulses events. Particle transport is dominated by the pressure head caused by the height of the fluid in the upper fluid cell. Pressure-driven flow is focused at the centre of the pore, encouraging alignment of the rods on-axis. This flow has been observed previously to produce a shear force capable of causing weakly interacting particles to dissociate at the pore mouth[26]. It might be expected that orientation effects were minimal in this work, because if a pore can allow a 2 μm sphere to pass through, this would imply that a 2.1 μm rod could traverse the pore in any orientation.

However, experimental FWHM values for rods are much larger than the modeled values. The most likely explanation for this is that rods do deviate from end-on orientation and can interact with each other and the pore walls, slowing the particles as they traverse the opening. Increased dwell time can also be explained by slower hydrodynamic motion of off-axis or tilted particles. This interpretation is supported by the long 'tail' of slow-moving particles evident for rods in the duration histogram, Figure 3D, which is responsible for the large differences in FWHM observed with the demonstration assay (Figure 5B). The orientation effect seems to be exaggerated as the length of the rod is increased, with the largest deviation from measured to modeled values appears at the FWHM for larger 4.7 μm rods. This interpretation is consistent with the previous hypothesis that, for rods, Δi_p increases at larger pore stretches due to a change in rod orientation. A skewed distribution is also evident for rods in the Δi_p histogram, Figure 3C

Although the model successfully predicts trends, orientation effects and the resulting skewed distributions (Figure 3 C, D) make it difficult to calculate exact durations. Regardless of whether the quantitative FWHM duration can be accurately predicted, this measurement provides a clear basis for distinguishing rod-like particles: despite the 2.1 μm rods possessing

a dimension similar to the 2 μm diameter sphere, the rod particles produce a significantly larger FWHM, Figure 3B. As the rod length is increased, the FWHM values also clearly increase.

3.2. Agglutination assay

Rods were then synthesized to contain a Ni segment, which was first conjugated to the avidin protein. Increasing the concentration of biotinylated-BSA in the solution caused two trends in the recorded values to be noted (Figure 7B). Firstly, both the Δi_p and FWHM values rose, the increase in signal continues to a concentration ~ 250 fM, before the number of binding sites on the particles start to become saturated, and a hook effect is observed[31]. Secondly, and more importantly, the FWHM is the dominant signal as the rods aggregate, forming longer particles. The increase in rod length, as demonstrated within the control assay, Figure 5B, resulted in FWHM changes that were much larger than those for Δi_p. The results from the side-on assay in Figure 7C show that an increase in analyte concentration caused a clear increase in Δi_p, whereas the FWHM did not change significantly. This side-on aggregation had the effect of forming rods with larger diameters but constant length. Similar behaviors were recorded for the PDGF assay using the end-on-end format. The sensitivity of the assay format is as low as 10 fM, 5 orders of magnitude lower than colorimetric assays[37] using the same capture probe. However the percentage change in both the FWHM and Δi_p is much lower than the example using avidin–biotin, indicating that fewer aggregates formed in the PDGF assay.

3.2.1 Assay sensitivity

The K_d for the PDGF aptamer and its target, is four orders of magnitude higher when compared to that of the avidin and biotin system. Therefore the smaller percentage changes in signal for the PDGF system is attributed to slower rates of reaction between the rod and

protein, which has been shown to be the rate limiting step in the formation of aggregates[34, 61]. To increase the rate of reaction either the particle size can be decreased, leading to enhanced mass transport, or the concentration of the particles can be increased, leading to higher collision and capture rates. Both factors are utilized here, the rods shaped particles may also have an advantage over spherical particles as they possess a planar surface to which the capture probe is anchored. This has recently been shown to enhance the association rates for triangular particles in DNA conjugation studies[62]. Once the analyte is captured onto the rod, residual magnetization of the Ni facilitated the formation of aggregates as the probability of two particles colliding and resulting in an aggregate is enhanced. This effect is shown in Figure 7A, which illustrates that particles over time formed non-specific aggregates through the magnetic interactions. The residual magnetization also has the effect of reducing the rate at which the particles separate. The force holding the particles together, F_A, is the sum of the force from the biological interaction, F_b, plus the magnetic interaction force, F_m[32] (calculated here to be 0.4pN[63]).

$$F_A = F_b + F_m \quad (2)$$

The sum of these two forces holds the particles together once a successful collision event has occurred, improving the sensitivity by prolonging the aggregate life time. This observation could help design agglutination assays for use in TPs.

The last factor which aids sensitivity is the measurement technique. Unlike detection formats such as light scattering or colorimetric assays, where the physical properties of the entire population of particles are measured simultaneously, with TPs each particles is measured independently as they traverse the pore, building a more representative measurement of the population. Whilst this technique has a lower throughput (circa 1000 particles a minute) and takes several minutes to record the data, it is potentially more accurate than ensemble techniques. A major benefit of TPs for aggregation assays is that the user can remove any

blockages that may occur during the assay by stretching the membrane, allowing larger aggregates to pass through the channel. Once the blockage has been removed the pore size can be returned back to its original size and the data collection continued.

4. Conclusions

The movement of rod shaped particles through TPs has been studied. It was demonstrated that as the rods traverse the pores, the resistive pulse magnitude is sensitive to the size of the particle, where as the FWHM values are a clear indication of the length. By increasing the length of the rod, a much longer FWHM translocation time is recorded. The orientation of rods passing through TPs can vary, significantly affecting resistive pulse data, particularly FWHM values. However, variations of rod orientation offer an intriguing additional parameter for monitoring particle behaviour. An agglutination assay based upon this observation was designed, whereby the resistive pulse magnitude or duration can be used as the indicator for analyte detection while controlling the orientation in which the rods come together. This was demonstrated using multicomponent rods composed of Ni and Au. The Ni segment can be selectively activated with a capture probe of interest, and act as a locus for aggregation. The control of the dominant signal created when rods aggregate, could make agglutination assays much easier to multiplex, as similar sized rods can be used for two different targets, simplifying particle synthesis. The sensitivity of the assay is aided by the multicomponent rods, and the residual magnetisation and is comparable to that of ELISA. The simple and fast format described here could be of benefit for point of care technologies.

Acknowledgements

This work was funded by an IEF Marie Curie fellowship grant FP7-PEOPLE-2009-IEF (252935). Support was provided by New Zealand's Ministry for Science and Innovation

(NERF contract C08X0806), and The Royal Society of New Zealand's International Mobility Fund (contract IMF10-B41), as well as Science Foundation Ireland (08/IN/2972).

5. Experimental Section

Chemicals and reagents. Phosphate buffered saline, PBS, (0.01 M phosphate buffer, 0.0027 M potassium chloride and 0.137 M sodium chloride, pH 7.4, P4417), Tween-20 (93773), Bovine serum albumin (A9085), Nickel Sulphate (227676), Boric acid (B7901), Sodium Dodecyl Sulphate (L4509), Ammonium Hydroxide (95313), Hydrogen Peroxide (95313), Methanol (34860), Ethanol (34870), Imidazole (I2399) were purchased from Sigma Aldrich. Sodium Hydroxide (S/4920/60) alumina foil (A/1570/50), and biotin-BSA (29130) were purchased from Fisher scientific. Avidin (A887), PDGF BB (PHG0046), Sulphate beads (1.96μm, CV < 2% F8853) were purchased from Invitrogen. Germany. Gold (42307) and Silver (44067) plating solutions were purchased from AlfaAeser. Anodisc 47 (6809-5012) were purchased from Whatman. SMCC (22360), and EDC (22980) were purchased from themo-fisher. Platinum wire (PT542201) and mesh (PT542501) used to construct the counter electrode were purchased from advent research materials. mPEG-SH, 1k (PLS-606) was purchased from creative PEG works. Peptide sequence HHHHHHGGSTGGSTGGKKK, was purchased from Mimotopes. Oigos FITC-NNNNNNNNN-Biotin, and the PDGF aptamer CAGGCTACGGCACGTAGAGCATCACCATGATCCTG-SH, were purchased from Entelechon. Ag/AgCl RE (K0265) was purchased from Princeton applied science.

Particle synthesis. Detailed synthesis strategies are outlined in full elsewhere[49]. A schematic of the process is shown in Figure 2. Electrochemical experiments were performed using a Princeton applied research Parstat 2273 with Powersuite software 2.58. Stage 1 - a 50nm layer of Ag was sputtered on to the filtration side of an alumina membrane. This

typically formed a silver layer but did not fully block the pores. Membranes were then placed into a silver plating solution and a charge of 7 C was passed by stepping to a potential of -1V versus the Ag/AgCl RE. Stage 2 - the membrane was placed into a holder and the uncoated side of the membrane exposed to the solution, the silver layer was placed in contact with a piece or alumina foil to make the contact with the potentiostat. Au was plated from a 1:5 dilution of stock plating solution at a potential of -0.95V versus the Ag/AgCl RE. Ni was deposited from a solution of 0.1M $NiSO_4$, 0.1M Boric acid and 5 mM SDS at a potential of -1.1V versus Ag/AgCl RE. Stage 3 – after deposition of the rod material the Ag layer was removed by soaking the membrane in a 4:1:1 solution of methanol:ammonium hydroxide:hydrogen peroxide for 30 mins. The alumina membrane was removed by placing it into 3 M NaOH for 2 hours. Particles were then collected through centrifugation at 10K rpm for 5 mins and washed three times with H_2O and three times with ethanol.

Surface chemistries. Particles which contained Ni segments were first washed with PBSTI (PBS, 0.1% tween-20, 0.1mM Imidazole) three times. Particles were then incubated in a solution of PBSTI containing 2 mg of peptide at room temperature for 2 hours. The solutions were placed on a rotating wheel and sonicated every 20 mins. After this stage the particles were collected with a hand held magnet and washed three times with PBST (PBS, 0.1% tween-20), then incubated in a solution of PBST containing 2 mg of PEG-SH on a rotating wheel for 2 hours, and sonicated every 20 mins. For particles only containing Au, the first peptide stage was omitted and the beads were immediately incubated with PEG-SH solution.

Conjugation to DNA and proteins. For conjugation of the peptide to avidin, 1mg of EDC was mixed with anAvidin solution at 2 mg/ml in PBST, and added to a rod solution of peptide modified rods. The solution was stirred for 90mins, and sonicated gently every 15 mins, before being washed with PBST three times. The result was Avidin functionalized Ni segments. For conjugation to DNA aptamers, 0.2mg of SMCC dissolved in DMSO was

added to a PBST solution of peptide modified rods. The rods were incubated with SMCC for 30 mins before being washed three times with PBST and re-suspended PBST, then 1nM of DNA was added to the solution.

Physical characterization. All magnetic properties were performed on a Quantum Design, magnetic properties measurement system, MPMS, Superconducting Quantum Interference Device. Scanning electron microscopy images, SEM, images were taken on a Hitachi S-4300 scanning electron microscope with accelerating voltage of 15kV. Optical Microscopy images were taken using a Zeiss observer Z1 microscope, 100x/1.41 Oil DIC III lens, and fluorescence images were taken suing a Filter Set 38HE (489038-9901-000)

Tunable pore measurements. TP measurements were made using the qNano system obtained from Izon Science (Christchurch), which incorporates the fluid cell, stretching apparatus, data recording and analysis software (v. 2.1) and the pore specimens themselves[8, 9]. The pores used were designated by 'NP1000' by the manufacturer, and therefore most suitable for detecting particles in the range 500 nm – 2000 nm. A pore stretch of 0 mm indicated the minimum stretch that can be applied, the maximum pore stretch is 8 mm. Typically a bandwidth filter of 1 kHz was applied during measurements, and mode values from the data sets are used in all plots. For calibration purposes, 955nm diameter spherical polystyrene particle standards were purchased from Izon and are shown in Figure S1.

References

[1] W.-J. Lan, D. A. Holden, J. Liu, H. S. White, *The Journal of Physical Chemistry C*, *115*, 18445.
[2] W.-J. Lan, D. A. Holden, B. Zhang, H. S. White, *Analytical Chemistry*, *83*, 3840.
[3] C. Dekker, *Nat Nano* **2007**, *2*, 209.
[4] T. Ito, L. Sun, R. R. Henriquez, R. M. Crooks, *Accounts of Chemical Research* **2004**, *37*, 937.
[5] R. R. Henriquez, T. Ito, L. Sun, R. M. Crooks, *Analyst* **2004**, *129*, 478.
[6] R. Vogel, G. Willmott, D. Kozak, G. S. Roberts, W. Anderson, L. Groenewegen, B. Glossop, A. Barnett, A. Turner, M. Trau, *Analytical Chemistry*, *83*, 3499.
[7] L. Sun, R. M. Crooks, *Journal of the American Chemical Society* **2000**, *122*, 12340.
[8] D. Kozak, W. Anderson, R. Vogel, M. Trau, *Nano Today*, *6*, 531.

[9] G. R. Willmott, R. Vogel, S. S. C. Yu, L. G. Groenewegen, G. S. Roberts, D. Kozak, W. Anderson, M. Trau, *Journal of Physics: Condensed Matter*, *22*, 454116.
[10] L. T. Sexton, L. P. Horne, C. R. Martin, *Molecular BioSystems* **2007**, *3*, 667.
[11] G. R. Willmott, M. F. Broom, M. L. Jansen, R. M. Young, W. M. Arnold, *Molecular and nano-tubes (Springer, Berlin, 2011). Tunable elastomeric pores* **2011**, *Ch 7*, 209.
[12] L. Song, M. R. Hobaugh, C. Shustak, S. Cheley, H. Bayley, J. E. Gouaux, *Science* **1996**, *274*, 1859.
[13] D. Branton, D. W. Deamer, A. Marziali, H. Bayley, S. A. Benner, T. Butler, M. Di Ventra, S. Garaj, A. Hibbs, X. Huang, S. B. Jovanovich, P. S. Krstic, S. Lindsay, X. S. Ling, C. H. Mastrangelo, A. Meller, J. S. Oliver, Y. V. Pershin, J. M. Ramsey, R. Riehn, G. V. Soni, V. Tabard-Cossa, M. Wanunu, M. Wiggin, J. A. Schloss, *Nat Biotech* **2008**, *26*, 1146.
[14] M. Rhee, M. A. Burns, *Trends in Biotechnology* **2007**, *25*, 174.
[15] O. A. Saleh, L. L. Sohn, *Nano Letters* **2002**, *3*, 37.
[16] R. An, J. D. Uram, E. C. Yusko, K. Ke, M. Mayer, A. J. Hunt, *Opt. Lett.* **2008**, *33*, 1153.
[17] L. J. Steinbock, G. Stober, U. F. Keyser, *Biosensors and Bioelectronics* **2009**, *24*, 2423.
[18] S. Lee, Y. Zhang, H. S. White, C. C. Harrell, C. R. Martin, *Analytical Chemistry* **2004**, *76*, 6108.
[19] G. S. Roberts, D. Kozak, W. Anderson, M. F. Broom, R. Vogel, M. Trau, *Small*, *6*, 2653.
[20] S. J. Sowerby, M. F. Broom, G. B. Petersen, *Sensors and Actuators B: Chemical* **2007**, *123*, 325.
[21] G. R. Willmott, P. W. Moore, *Nanotechnology* **2008**, *19*, 475504.
[22] R. Vogel, W. Anderson, J. Eldridge, B. Glossop, G. R. Willmott, *submitted* **2011**.
[23] G. S. Roberts, S. Yu, Q. Zeng, L. C. L. Chan, W. Anderson, A. H. Colby, M. W. Grinstaff, S. Reid, R. Vogel, *Biosensors and Bioelectronics*.
[24] M. Low, S. Yu, M. Y. Han, X. Su, *Aust. J. Chem.* **2011**, *64*, 1229.
[25] G. R. Willmott, B. E. T. Parry, *Journal of Applied Physics*, *109*, 094307.
[26] G. R. Willmott, M. Platt, G. U. Lee, *Biomicrofluidics* **2012**, *article accepted*.
[27] N. Pamme, *Lab on a Chip* **2007**, *7*, 1644.
[28] N. Pamme, C. Wilhelm, *Lab on a Chip* **2006**, *6*, 974.
[29] J. H. Chang, H. Shang, R. M. Perera, S.-m. Lok, D. Sedlak, R. J. Kuhn, G. U. Lee, *Analyst* **2008**, *133*, 233.
[30] S. Giri, E. A. Sykes, T. L. Jennings, W. C. W. Chan, *ACS Nano*, *5*, 1580.
[31] M. Platt, J. Muzard, G. U. Lee, G. Cannon, M. Carr, P. Li, *Submitted*

[32] S. Y. Park, H. Handa, A. Sandhu, *Nano Letters* **2009**, *10*, 446.
[33] B.-K. Oh, S. Park, J. E. Millstone, S. W. Lee, K.-B. Lee, C. A. Mirkin, *Journal of the American Chemical Society* **2006**, *128*, 11825.
[34] J. Baudry, C. Rouzeau, C. Goubault, C. Robic, L. Cohen-Tannoudji, A. Koenig, E. Bertrand, J. Bibette, *Proceedings of the National Academy of Sciences* **2006**, *103*, 16076.
[35] S. Y. Park, P. J. Ko, H. Handa, A. Sandhu, *Journal of Applied Physics*, *107*, 09B324.
[36] B. B. Yellen, R. Erb, m., H. Son, S., R. Hewlin, H. Shang, G. U. Lee, *Lab chip* **2007**, *7*, 1681.
[37] C.-C. Huang, Y.-F. Huang, Z. Cao, W. Tan, H.-T. Chang, *Analytical Chemistry* **2005**, *77*, 5735.

[38] J.-Y. Chang, H. Wu, H. Chen, Y.-C. Ling, W. Tan, *Chemical Communications* **2005**, 1092.
[39] A. Ranzoni, J. J. H. B. Schleipen, L. J. van Ijzendoorn, M. W. J. Prins, *Nano Letters*, *11*, 2017.
[40] C. Shad Thaxton, R. Elghanian, A. D. Thomas, S. I. Stoeva, J.-S. Lee, N. D. Smith, A. J. Schaeffer, H. Klocker, W. Horninger, G. Bartsch, C. A. Mirkin, *Proceedings of the National Academy of Sciences* **2009**.
[41] N. L. Rosi, C. A. Mirkin, *Chemical Reviews* **2005**, *105*, 1547.
[42] K. P. Yuet, D. K. Hwang, R. Haghgooie, P. S. Doyle, *Langmuir* **2009**, *26*, 4281.
[43] S.-N. Yin, C.-F. Wang, Z.-Y. Yu, J. Wang, S.-S. Liu, S. Chen, *Advanced Materials*, *23*, 2915.
[44] R. M. Erb, N. J. Jenness, R. L. Clark, B. B. Yellen, *Advanced Materials* **2009**, *21*, 4825.
[45] K.-H. Roh, D. C. Martin, J. Lahann, *Nat Mater* **2005**, *4*, 759.
[46] D. Dosev, M. Nichkova, R. K. Dumas, S. J. Gee, B. D. Hammock, K. Liu, I. M. Kennedy, *Nanotechnology* **2007**, *18*, 055102.
[47] M. Abe, T. Suwa, *Physical Review B* **2004**, *70*, 235103.
[48] J. Nam, C. Thaxton, C. Mirkin, *Science* **2003**, *301*, 1884
[49] M. J. Banholzer, L. Qin, J. E. Millstone, K. D. Osberg, C. A. Mirkin, *Nat. Protocols* **2009**, *4*, 838.
[50] Y. Cao, R. Jin, J. Nam, C. Thaxton, C. Mirkin, *JACS* **2003**, *125*, 14676
[51] S. R. Nicewarner-PeÃ±a, R. G. Freeman, B. D. Reiss, L. He, D. J. PeÃ±a, I. D. Walton, R. Cromer, C. D. Keating, M. J. Natan, *Science* **2001**, *294*, 137.
[52] C. R. Martin, *Science* **1994**, *266*, 1961.
[53] K. K. Caswell, J. N. Wilson, U. H. F. Bunz, C. J. Murphy, *Journal of the American Chemical Society* **2003**, *125*, 13914.
[54] A. Gole, C. J. Murphy, *Langmuir* **2005**, *21*, 10756.
[55] C. G. Knight, M. Platt, W. Rowe, D. C. Wedge, F. Khan, P. J. R. Day, A. McShea, J. Knowles, D. B. Kell, *Nucleic Acids Research* **2009**, *37*, e6.
[56] M. Platt, W. Rowe, D. C. Wedge, D. B. Kell, J. Knowles, P. J. R. Day, *Analytical Biochemistry* **2009**, *390*, 203.
[57] A. Ellington, J. Szostak, *Nature* **1990**, *346*, 818
[58] A. Ortega, J. G. d. l. Torre, *The Journal of Chemical Physics* **2003**, *119*, 9914.
[59] M. A. Castanho, W. Brown, M. J. Prieto, *Biophysical Jounral* **1992**, *63*, 1455.
[60] D. Lehner, H. Lindner, O. Glatter, *Langmuir* **2000**, *16*, 1689.
[61] L. Cohen-Tannoudji, E. Bertrand, J. Baudry, C. Robic, C. Goubault, M. Pellissier, A. Johner, F. Thalmann, N. K. Lee, C. M. Marques, J. Bibette, *Physical Review Letters* **2008**, *100*, 108301.
[62] M. R. Jones, R. J. Macfarlane, A. E. Prigodich, P. C. Patel, C. A. Mirkin, *Journal of the American Chemical Society*, *133*, 18865.
[63] D. Vokoun, M. Beleggia, L. k. Heller, P. Å ittner, *Journal of Magnetism and Magnetic Materials* **2009**, *321*, 3758.

Submitted to small

Received: ((will be filled in by the editorial staff))

Revised: ((will be filled in by the editorial staff))

Published online on ((will be filled in by the editorial staff))

Figures

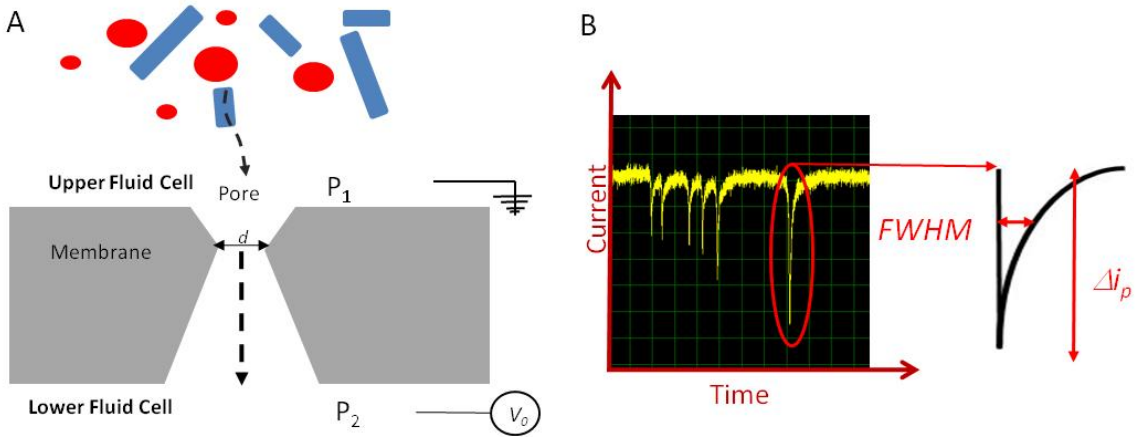

Figure 1. Overview of the nanopore detection process. A – Schematic of the nanopore. The sample is placed into the upper fluid cell. B – Example of baseline current and "blockade" events (dips in current) that are caused by translocation events. Each blockade event is analysed for full width half maximum, FWHM, and Δi_p.

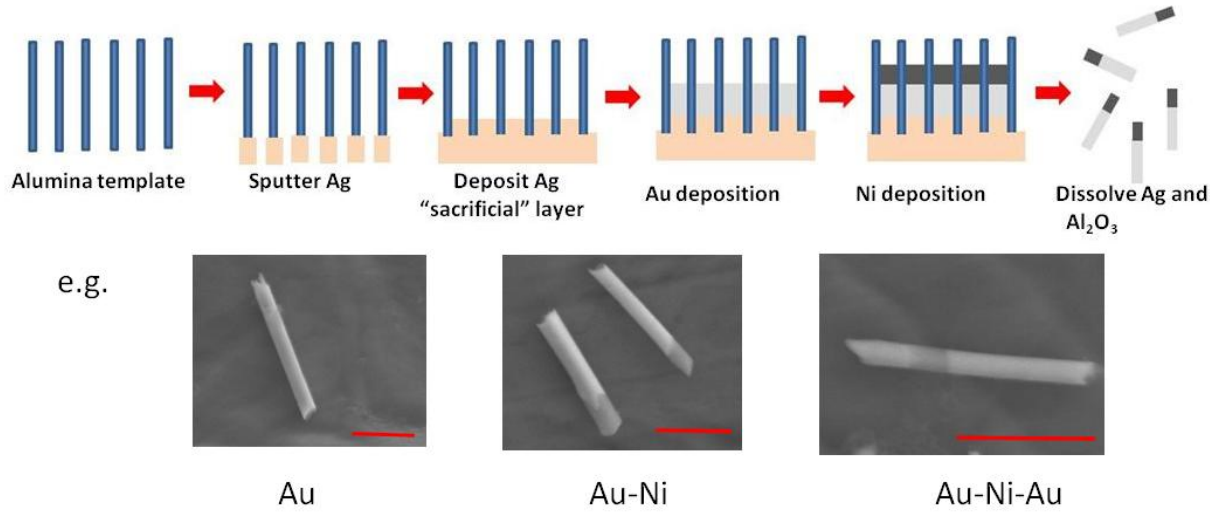

Figure 2 Schematic of the particle synthesis. An Alumina membrane is sputtered with a layer of Ag which acts as the electrode. First the pores are filled with a sacrificial silver layer, followed by layers of Au and Ni. The particles are released from the alumina by dissolution of the Ag and Al_2O_3. Examples of the composition of particles used in this study are shown below, Au rods (left) Au-Ni (middle) and Au-Ni-Au (right). Scale bar = 0.5μm.

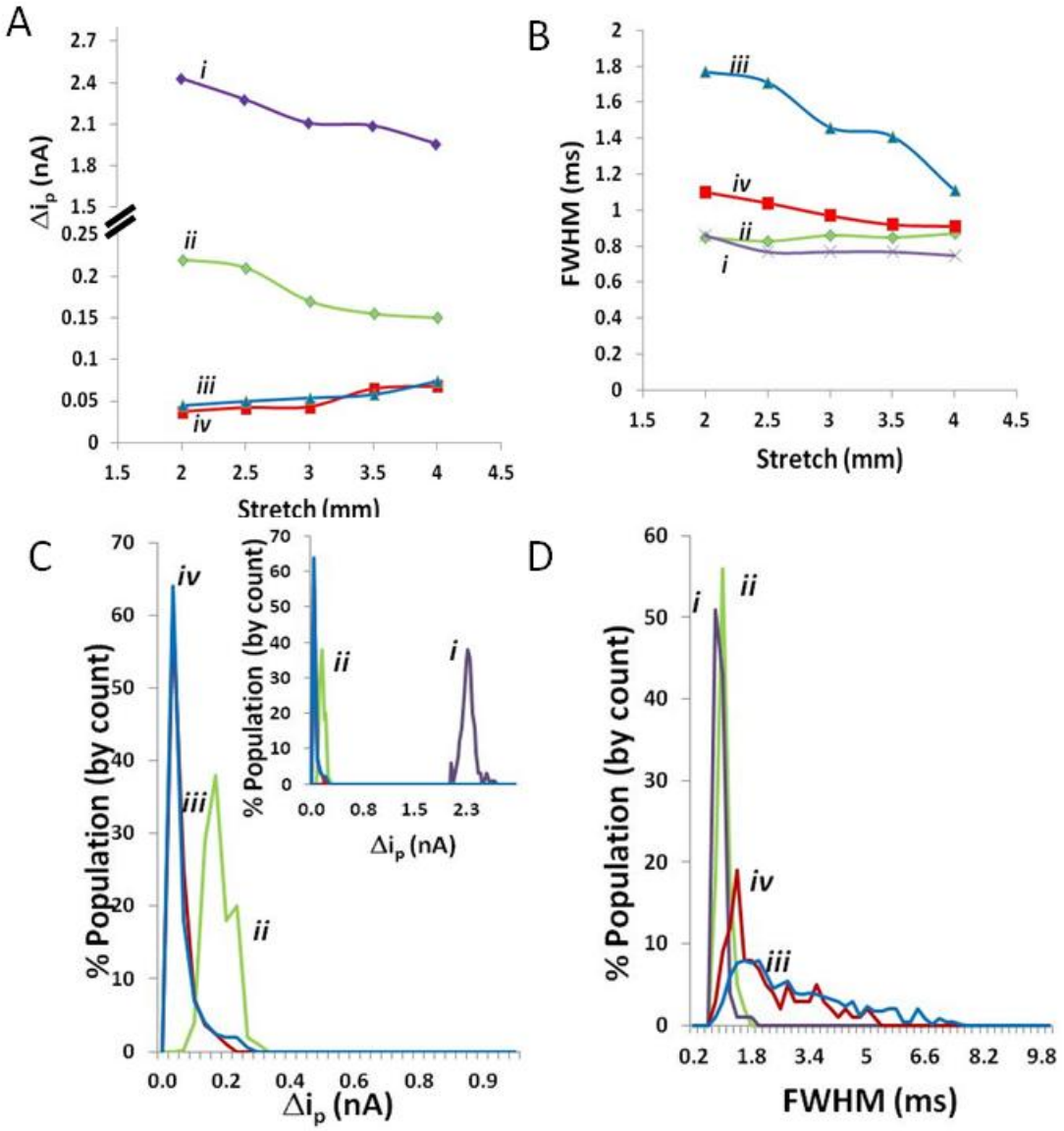

Figure 3. Purple (i)= sphere (2 μm diameter), Green(ii) = sphere (0.955 μm diameter), blue(iii) = Au rod (4.7 μm length-CV 14%, 290 nm diameter-CV 15%), Red (iv)=Au rod (2.15 μm length-CV 20%, 325 nm diameter-CV 14%). A, Modal Δi_p values as pore size is varied, fixed potential of 0.12V, B, Modal FWHM values as pore size is varied, fixed potential of 0.12V. C, Δi_p histogram for the samples run at a stretch of 2.5mm in part A. D FWHM histogram for samples run at a stretch of 2.5mm part B.

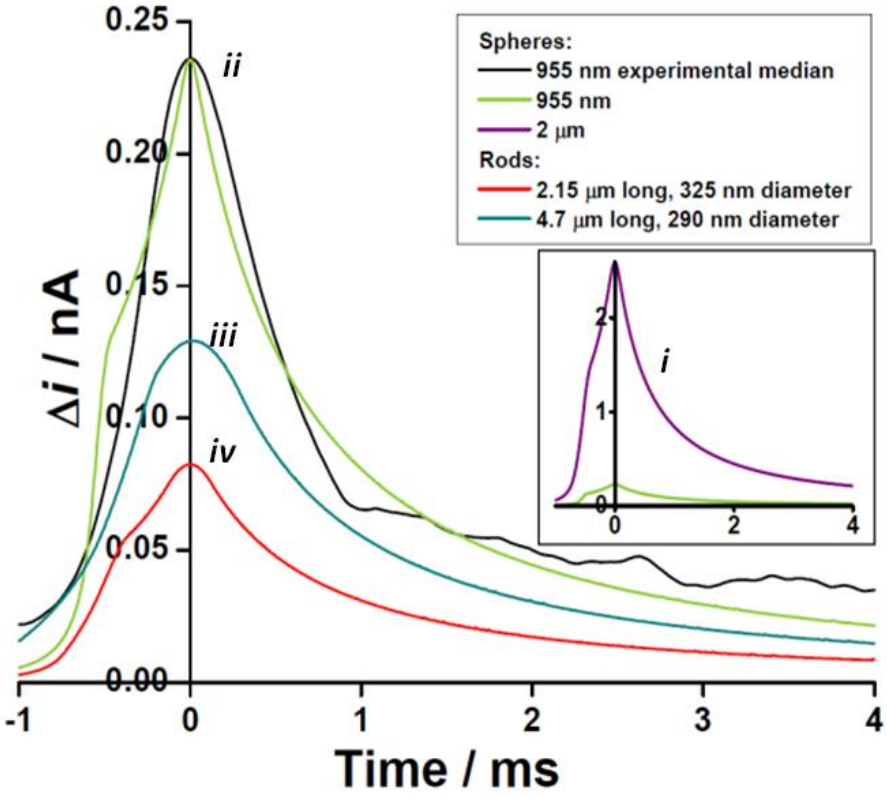

Figure 4. Simulated resistive pulses for the particles studied in Figure. 3, Purple (i)= sphere (2 μm diameter), Green(ii) = sphere (0.955 μm diameter), blue(iii) = Au rod (4.7 μm length-CV 14%, 290 nm diameter-CV 15%), Red (iv)=Au rod (2.15 μm length-CV 20%, 325 nm diameter-CV 14%). Ccalibrated using data for 955 nm spheres at X = 2.5 mm and 0.12 V. Inset: An expanded vertical axis allows comparison with the simulation for a 2 μm sphere.

	Δi_p (nA)		FWHM (ms)	
	Simulated	Measured	Simulated	Measured
2 μm Sphere	0.24	0.21	1.06	0.83
0.955 μm Sphere	2.59	2.28	1.01	0.77
2.1 μm Rod	0.08	0.05	1.13	0.91
4.17 μm Rod	0.13	0.06	1.30	1.90

Table 1. Measured and simulated values for the Dip and FWHM, using a potential of 0.12V and a stretch of 2.5 mm.

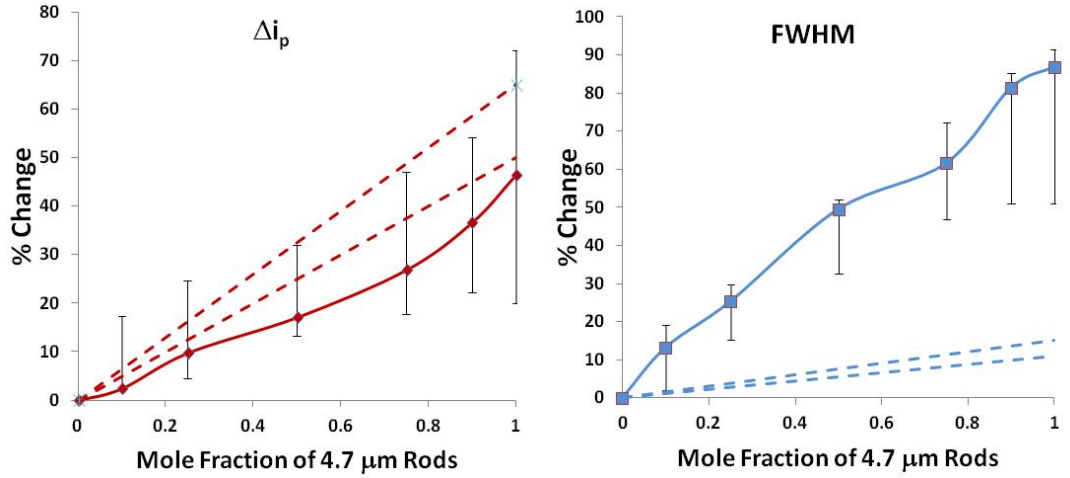

Figure 5. Changes in Δi_p, and FWHM, as mole fraction of 4.7 μm rods is increased. Dashed lines join the maximum and minimum values predicted by simulations for 0% and 100% molar fraction, given the CV of the particle set size distribution. Error bars show the d25 and d75, values for each data point.

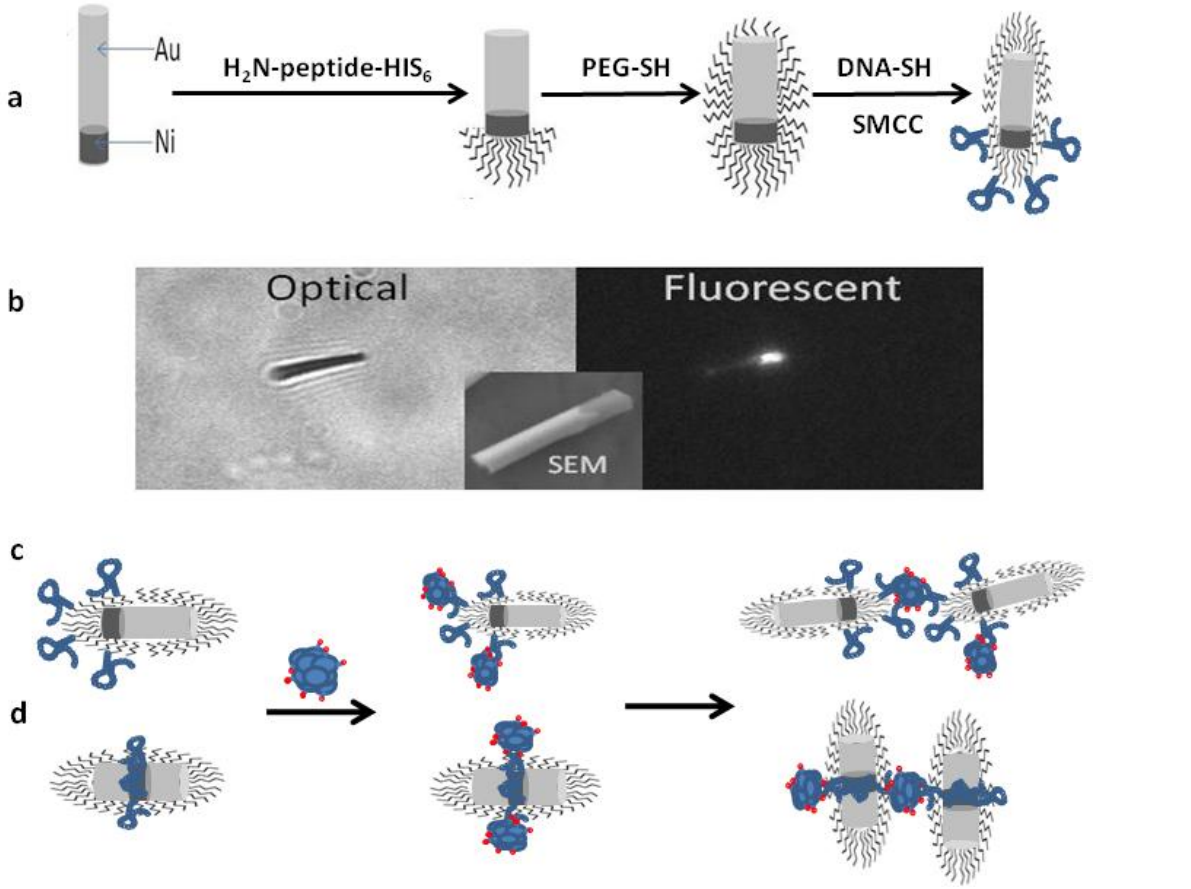

Figure 6, a- Overview of the surface chemistry modifications and assays. a - The surfaces of the Ni segments are modified with a His-tagged peptide, the Au segments are modified with PEG-SH molecules. b – Confirmation of localised surface chemistries with fluorescent modified Ni segments. c – Schematic of the aggregation assay via "end-on-end" aggregation d – Schematic of the aggregation assay via "Side-on" aggregation

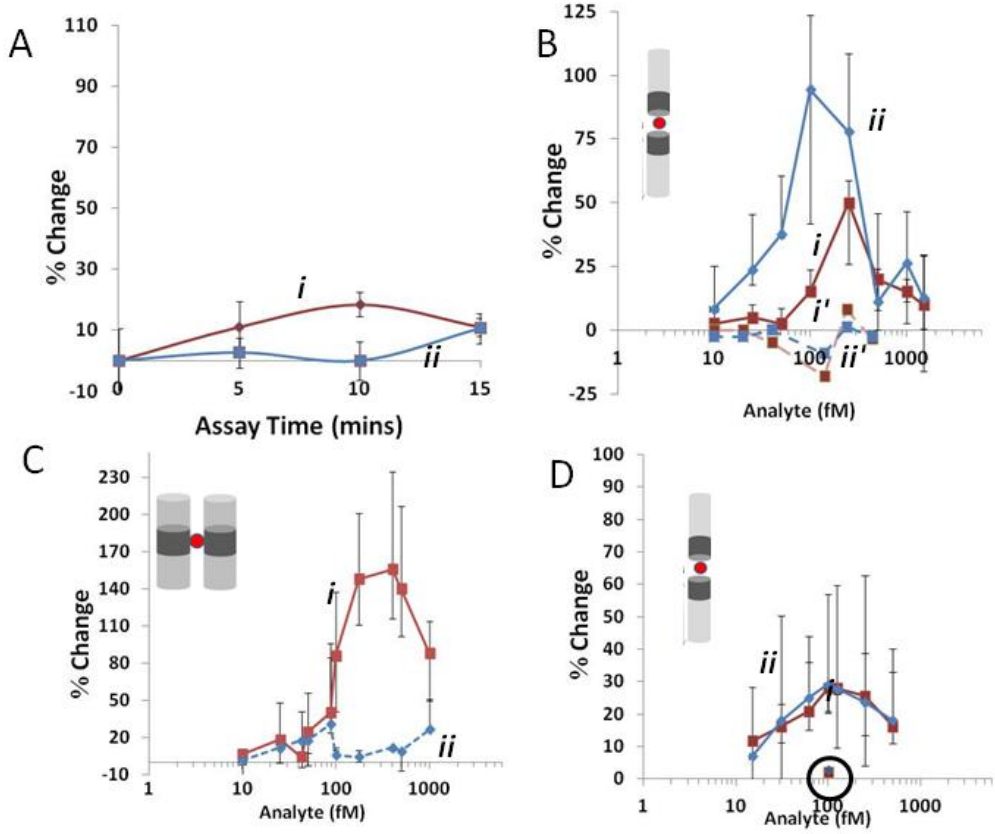

Figure 7. Performed using a NP1000, stretch=2.5mm, Potential =0.14, red (i) indicate Δi_p, blue (ii) indicate FWHM. A, AuNi rods, 1.23 μm in length (CV 20%, Ni content 15% by length), 400fM, % Change Δi_p and FWHM as assay time is increased in the absence of an analyte. B, Same rods as A, assay time 10 mins. Ni segments functionalised with Avidin. Dashed lines represent a 10 min assay with a non biotinylated target. C, AuNiAu rods, 0.82 μm in length (CV 14%, Ni content 18% by length), 500 fM, assay time 10 mins. D, AuNi rods, 1.1 μm in length (CV 20%, Ni content 14% by length), 150fM assay time 10 mins. Ni segments functionalised with PDGF aptamer. The circles data points plotted at 100fM indicate the change in FWHM and Δip for the same rods using a control protein. Error bars show the d25 and d75, values for each data point.

.

The table of contents entry

Tunable nanopores, *TPs,* are used to monitor individual and aggregated rod shaped nanoparticles as they move through a membrane opening. By controlling the surface chemistry and the location of the capture ligand, rods were made to form either long "end-on-end" or wide "side-on" aggregates upon the addition of an analyte. We demonstrate the assay's potential with sensitivities down to femtomolar levels.

Keywords - Tunable pores, multicomponent rods, aptamer, agglutination, platelet derived growth factor

Mark Platt, Geoff R. Willmott and Gil U. Lee

Investigation of analyte-induced multicomponent rod aggregation using tunable pores